Shadows in dyonic Kerr-Sen black holes

Soumya Jana[1,2,∗] and Sayan Kar[2,†]

[1]*Department of Physics, Sitananda College, Nandigram, 721631, India*

[2]*Department of Physics, Indian Institute of Technology, Kharagpur - 721302, India*

Abstract

Black holes with dyonic charges in Einstein-Maxwell-dilaton-axion supergravity theory are revisited in the context of black hole shadows. We consider static as well as rotating (namely the dyonic Kerr-Sen) black holes. The matter stress-energy tensor components, sourced by the Maxwell, axion and dilaton fields satisfy the standard energy conditions. The analytical expressions for the horizon and the shadow radius of the static spacetimes demonstrate their dependence on $P^2 + Q^2$ (P, Q the magnetic and electric charges, respectively) and the mass parameter M. The shadow radius lies in the range $2M < R_{shadow} < 3\sqrt{3}M$ and there is no stable photon orbit outside the horizon. Further, shadows cast by the rotating dyonic Kerr-Sen black holes are also studied and compared graphically with their Kerr-Newman and Kerr-Sen counterparts. Deviation of the shadow boundary is prominent with the variation of the magnetic charge, for the relatively slowly rotating dyonic Kerr-Sen spacetimes. We test any possible presence of a magnetic monopole charge in the backdrop of recent EHT observations for the supermassive black holes M87* and Sgr A*. Deviation from circularity of the shadow boundary (ΔC) and deviation of the average shadow radius from the Schwarzschild shadow radius (quantified as the fractional deviation parameter δ) are the two observables used here. Observational bound on ΔC (available only for M87*) is satisfied for all theoretically allowed regions of parameter space and thus cannot constrain the parameters. The observational bound on δ available for Sgr A* translates into an upper limit on any possible magnetic monopole charge linked to Sgr A* and is given as $P \lesssim 0.873\,M$. Such a constraint on P is however expected to be far more stringent for other astrophysical tests.

∗ Email Address: soumyajana.physics@gmail.com

† Email Address: sayan@phy.iitkgp.ac.in

I. INTRODUCTION

The Reissner–Nordstrom (RN) geometry representing the gravitational field due to a charged massive object is among the earliest known exact solutions in General Relativity coupled to electromagnetism, i.e. the Einstein–Maxwell theory. A straightforward generalisation of this solution is the dyonic RN spacetime [1] which can be written down by just replacing the Q^2 in RN spacetime with $P^2 + Q^2$, where P represents the 'magnetic' charge and Q is its 'electric' counterpart. However, for the dyonic solution, the definition of the electromagnetic potential A_i is a little tricky –one needs, as expected for a dyon, a two-patch definition – one for the northern hemisphere and the other for the southern. The standard electric-magnetic duality which arises when both magnetic and electric charges are present keeps the solution unchanged. The horizons and other features for the dyonic RN spacetime resemble those for the usual RN geometry modulo the presence of the extra magnetic charge.

It is also known that additional matter fields (other than Maxwell) such as the dilaton and/or the axion appear in the context of supergravity theories or in low energy effective actions which emerge out of full string theory [2–4]. In such scenarios too one expects dyonic solutions representing gravitational fields of such objects. Among various known solutions [2–7] there are static, spherically symmetric ones as well stationary spacetimes wherein rotation is present. The purpose of this article is to revisit such known solutions without and with rotation. Our primary aim is to learn how the various theory parameters (eg. electric, magnetic as well as other charges) control the nature and profile of the shadow/silhouette created by the gravitational field representing such solutions. We also try and see if any meaningful constraint can be placed on the various charges, using the known shadow observations for the supermassive compact object present in M87* [8–10] and for Sgr A* [11, 12]. Though, dyonic scenarios presently have little to do with observations in other contexts, we will see how one may place bounds on their viability through shadow observations. In other words, we try to show that what is seen in the images may also be explained using hypothetical constructs which, by no means can be ruled out altogether, unless other observations imply mismatches and contradictions.

Shadows in Kerr-Sen Black holes [4] have already been studied by several authors [13–15]. The rotating version of the dyonic black holes in Einstein-Maxwell-dilaton theory [2, 16] and its shadows were studied in [17]. In [18], the authors investigated shadows

2

of regular (Bardeen) black holes having magnetic monopole charge sourced by nonlinear electrodynamics coupled to GR. Presence of axionic hair or the Kalb-Ramond field and their influence on the shadow of M87* was investigated in [19].

Our article is organised as follows. In Section II we recall the static black hole solutions and discuss the energy conditions in Einstein-Maxwell–dilaton-axion (EMDA) supergravity theory. Section III provides a summary of the corresponding stationary solutions (dyonic) which include rotation. Shadow calculations and related details are presented in Section IV and connections/comparisons with observations are outlined in Section V. The final Section VI is a summary with concluding remarks.

II. BLACK HOLES IN EINSTEIN -MAXWELL- DILATON-AXION SUPER-GRAVITY THEORY

The Einstein-Maxwell -Dilaton- Axion (EMDA) supergravity theory is described by the action [6]

$$S_{\text{EMDA}} = \int d^4x \sqrt{-g} \left[R - \frac{1}{2}(\partial\Phi)^2 - \frac{1}{2}e^{2\Phi}(\partial\xi)^2 - e^{-\Phi}F^2 + \xi F_\mu \tilde{F}^{\mu\nu} \right] \tag{2.1}$$

where Φ and ξ are the dilaton and axion fields, $F_{\mu\nu}$ is the usual electromagnetic field tensor, $F^2 = F_{\mu\nu}F^{\mu\nu}$, and $\tilde{F}^{\mu\nu} = \frac{1}{2\sqrt{-g}}\epsilon^{\mu\nu\alpha\beta}F_{\alpha\beta}$ is the dual electromagnetic field tensor. The equations of motion of the dilaton, axion fields are obtained as

$$\Box\Phi - e^{2\Phi}(\partial\xi)^2 + e^{-\Phi}F^2 = 0, \tag{2.2}$$

and

$$\Box\xi + 2\nabla^\mu\Phi\nabla_\mu\xi + e^{-2\Phi}F_{\mu\nu}\tilde{F}^{\mu\nu} = 0. \tag{2.3}$$

The equation of motion for the electromagnetic vector potential A_μ (where $F_{\mu\nu} = \partial_\mu A_\nu - \partial_\nu A_\mu$) is obtained as

$$\nabla_\mu \left(-e^{-\Phi}F^{\mu\nu} + \xi\tilde{F}^{\mu\nu} \right) = 0, \tag{2.4}$$

along with the usual Bianchi identity,

$$\nabla_\mu\tilde{F}^{\mu\nu} = 0. \tag{2.5}$$

The equation of motion for the metric tensor $g_{\mu\nu}$ is obtained by varying the action (2.1) with respect to $g_{\mu\nu}$. We get

$$R_{\mu\nu} = \frac{1}{2}\nabla_\mu\nabla_\nu\Phi + \frac{1}{2}e^{2\Phi}\nabla_\mu\xi\nabla_\nu\xi + 2e^{-\Phi}F_{\mu\alpha}F_\nu{}^\alpha - \frac{1}{2}g_{\mu\nu}e^{-\Phi}F^2, \tag{2.6}$$

where $R_{\mu\nu}$ are the Ricci tensor components.

A. Static Black Hole solution

The static black hole solution in such a system has already been obtained in [6], where the authors used symmetry transformations on the axion and dilaton fields to obtain its form. In this section, we first outline the derivation of the same solution by solving directly, the Einstein field equations. Thereafter, we analyze the structure of the black hole solution.

We consider the ansatz for the spherically symmetric static line element

$$ds^2_{static} = -\Delta^2(R)dt^2 + \frac{\psi^2(R)}{\Delta^2(R)}dR^2 + R^2\left(d\theta^2 + \sin^2\theta d\phi^2\right). \tag{2.7}$$

We also assume nonvanishing components of the electromagnetic field tensor

$$F_{01} = -F_{10} = \mathcal{E}(R), \qquad F_{23} = -F_{32} = \mathcal{B}(R)\sin\theta. \tag{2.8}$$

Then the Eq. (2.4) becomes

$$\left(\frac{e^{-\Phi}\mathcal{E}R^2}{\psi} + \xi\mathcal{B}\right)' = 0, \tag{2.9}$$

where the prime $(')$ denotes the derivative with respect to the radial coordinate R. The Bianchi identity is satisfied for $\mathcal{B}(R) = P$ (a constant) and P is therefore identified as the magnetic charge since

$$\tilde{F}^{10} = -\frac{P}{R^2\psi}. \tag{2.10}$$

Integrating Eq. (2.9), we get

$$\mathcal{E} = \psi e^\Phi \left(\frac{Q - \xi P}{R^2}\right), \tag{2.11}$$

where the integration constant Q is identified as the electric charge, since, at large R, $\mathcal{E} \sim Q/R^2$. The equations of motion [Eqs.(2.2)-(2.3)] for the dilaton and the axion field become

$$\left(\frac{\Delta^2 R^2 \Phi'}{\psi}\right)' = 2e^{-\Phi}\psi R^2 \left(\frac{\mathcal{E}^2}{\psi^2} - \frac{P^2}{R^4}\right) + e^{2\Phi}\frac{R^2\Delta^2}{\psi}\xi'^2, \tag{2.12}$$

and

$$\left(\frac{\Delta^2 R^2 \xi'}{\psi}\right)' = -2\frac{\Delta^2 R^2}{\psi}\Phi'\xi' - 4e^{-2\Phi}P\mathcal{E}. \tag{2.13}$$

4

Note from Eq. (2.13) that for $\xi = 0$, $P = 0$ or $Q = 0$. From Eq. (2.6), we get three non-vanishing components which are

$$R_{00} = \frac{\Delta^4}{\psi^2}\left[\frac{\Delta'^2}{\Delta^2} - \frac{\Delta'\psi'}{\Delta\psi} + \frac{(\Delta'R^2)'}{\Delta R^2}\right] = e^{-\Phi}\Delta^2\left(\frac{\mathcal{E}^2}{\psi^2} + \frac{P^2}{R^4}\right), \tag{2.14}$$

$$R_{11} = \frac{2\psi'}{R\psi} - \frac{\Delta'^2}{\Delta^2} + \frac{\Delta'\psi'}{\Delta\psi} - \frac{(\Delta'R^2)'}{\Delta R^2} = \frac{1}{2}\Phi'^2 + \frac{1}{2}e^{2\Phi}\xi'^2 - e^{-\Phi}\frac{\psi^2}{\Delta^2}\left(\frac{\mathcal{E}^2}{\psi^2} + \frac{P^2}{R^4}\right), \tag{2.15}$$

$$R_{22} = 1 - 2R\frac{\Delta\Delta'}{\psi^2} + \frac{\Delta^2 R^2}{\psi^3}\left(\frac{\psi}{R}\right)' = R^2 e^{-\Phi}\left(\frac{\mathcal{E}^2}{\psi^2} + \frac{P^2}{R^4}\right). \tag{2.16}$$

Using Eqs. (2.14) and (2.15), we get

$$\frac{2}{R}\frac{\psi'}{\psi} = \frac{1}{2}\Phi'^2 + \frac{1}{2}e^{2\Phi}\xi'^2. \tag{2.17}$$

Demanding proper asymptotic behaviour, i.e. $\Phi \to 0$ and $\xi \to 0$, $\psi \to 1$ for $R \to \infty$, we assume,

$$\frac{\psi'}{\psi} = \frac{\sigma^2}{R(R^2 + \sigma^2)}, \quad \text{or,} \quad \psi^2 = \frac{R^2}{R^2 + \sigma^2}, \tag{2.18}$$

where σ^2 is a constant. From Eqs. (2.14) and (2.16), we get

$$\left[\frac{1}{2}\frac{(\Delta^2 R^2)'}{\psi}\right]' = \psi. \tag{2.19}$$

Solving this equation with the assumption on ψ given in Eq. (2.18), we obtain the solution for $\Delta(r)$ as

$$\Delta^2(R) = 1 - \frac{2M\sqrt{R^2 + \sigma^2}}{R^2} + \frac{P^2 + Q^2}{R^2}, \tag{2.20}$$

where the integration constants are identified as the mass M and the sum of the square of the charges $(P^2 + Q^2)$. The black hole resembles the Reissner-Nordström black holes asymptotically. Using the Eqs. (2.18) and (2.20) the solution for the equations of motion for the dilaton and axion fields are

$$e^{\Phi} = 1 + \frac{2d}{R^2}\sqrt{R^2 + k^2 + d^2} + \frac{2(k^2 + d^2)}{R^2}, \tag{2.21}$$

$$\xi = \frac{2k\sqrt{R^2 + k^2 + d^2}}{R^2 + 2d\sqrt{R^2 + k^2 + d^2} + 2(k^2 + d^2)}, \tag{2.22}$$

where, $d = \frac{(P^2 - Q^2)}{2M}$ and $k = \frac{PQ}{M}$ are dilaton and axion charges respectively and $\sigma^2 = k^2 + d^2$.

In the absence of both electric and magnetic charges (i.e. $P = Q = 0$), the dyonic and axionic charges also vanish, i.e. $k = d = 0$, and we recover the Schwarzschild black hole. For any non-zero P and/or Q, the line element does not resemble the Riessner-Nordström

black holes. This signifies that these black holes are hairy. Another distinguishing feature of these black holes are that they have single horizons – unlike the Riessner-Nordström. Using the relation $k^2 + d^2 = (P^2 + Q^2)^2 / 4M^2$ in the $f(R_{hz}) = 0$, we get the horizon radius as,

$$R_{hz} = 2M\sqrt{1 - \frac{P^2 + Q^2}{2M^2}}. \tag{2.23}$$

This feature is also different from Riessner-Nordström and the dyonic black holes with dilaton field as the only scalar hair. We notice a double horizon in general and extremal horizon in a special situation. However, the static version of the Kerr-Sen black holes share the similar feature of a single horizon. For black holes,

$$M \geq \sqrt{\frac{P^2 + Q^2}{2}}, \tag{2.24}$$

otherwise, we have naked singularities. This is illustrated in Fig. 1.
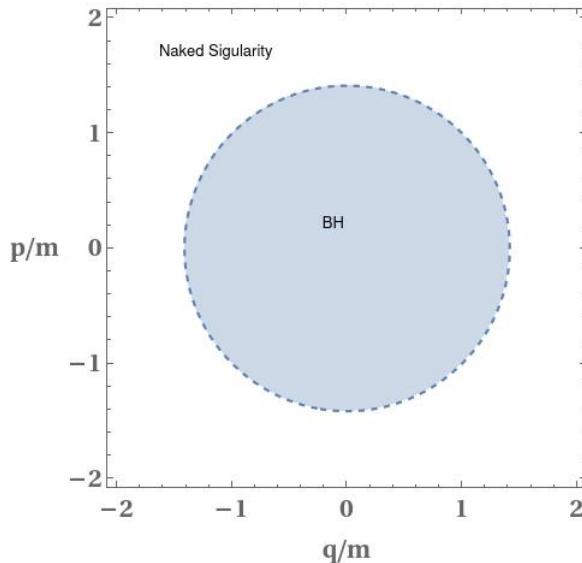

FIG. 1: $\frac{P}{M}$ vs. $\frac{Q}{M}$ parameter space is plotted. The shaded circular region indicates the allowed parameter space for black holes and the exterior region in parameter space corresponds to naked singularities.

B. Energy conditions

By identifying the non-zero components of the stress-energy tensors as $T^0{}_0 = -\rho$, $T^1{}_1 = \tau$, and $T^2{}_2 = T^3{}_3 = p$, where ρ (energy density), τ (radial pressure), and p (tangential

pressure) are defined in the orthonormal frame basis, and using the Einstein field equations ($T_{\mu\nu} = G_{\mu\nu}/8\pi G$), we analyze all the energy conditions. We find that:

(a) The Null Energy Conditions (NEC), i.e. $\rho + \tau \geq 0$ and $\rho + p \geq 0$ are satisfied when $\Delta^2(R) \geq 0$. This implies that the NEC is satisfied on and outside the horizon of the black hole. For a naked singularity, the NEC is satisfied for all R.

(b) The Weak Energy Conditions (WEC) implies $\rho \geq 0$ in addition to the NEC. Using the Einstein field equation

$$\rho = \frac{1}{8\pi G}\left[\frac{1}{R^2} - \frac{(\Delta^2)'}{R\psi^2} - \frac{\Delta^2}{R^2\psi^2} + 2\frac{\Delta^2\psi'}{R\psi^3}\right]. \tag{2.25}$$

One can check that $\rho \geq 0$ for $R \geq R_{hz}/\sqrt{3}$ for black holes, and for all R in case of naked singularities. Thus, the WEC is also satisfied on and outside the horizon of the black holes.

(c) The Strong Energy Condition (SEC), i.e. $\rho + \tau + 2p \geq 0$ is satisfied for all R irrespective of black holes or naked singularities.

(d) The Dominant Energy Conditions (DEC), i.e. $\rho \geq 0$, $\rho \geq |\tau|$, and $\rho \geq |p|$ are satisfied on and outside of the black hole horizon, and for all R in case of naked singularities.

It was conjectured [20], [21] that "a violation of either the dominant or the strong energy condition is a necessary condition for the existence of an anti-photon sphere outside a regular black hole horizon". Thus, according to our analysis of the energy conditions, the static dyonic black holes in the EMDA theory do not consist anti-photon sphere or stable photon orbits.

III.   DYONIC KERR-SEN BLACK HOLES

Dyonic Kerr-Sen black holes are the rotating versions of the static black holes. The Newman-Janis (NJ) algorithm [22, 23] can be applied to obtain such rotating black holes. After introducing a new radial coordinate r such that the squared area radius $R^2 = r^2 - 2dr - k^2$ or $r = \sqrt{R^2 + k^2 + d^2} + d$, the static line element (2.7,2.18, 2.20) becomes

$$ds^2 = -f(r)dt^2 + \frac{dr^2}{g(r)} + h(r)\left(d\theta^2 + \sin^2\theta d\phi^2\right), \tag{3.1}$$

where

$$f(r) = g(r) = 1 - \frac{2M(r-d) - P^2 - Q^2}{r^2 - 2dr - k^2}$$
$$= \left(1 - \frac{2(d+M)}{r} + \frac{2P^2 - k^2}{r^2}\right)\left(1 - \frac{2d}{r} - \frac{k^2}{r^2}\right)^{-1}, \tag{3.2}$$

and

$$h(r) = R^2(r) = r^2 - 2dr - k^2$$
$$= r^2 \left(1 - \frac{2d}{r} - \frac{k^2}{r^2} \right). \tag{3.3}$$

In terms of the advanced Eddington-Finkelstein coordinates (u, r, θ, ϕ), where $du = dt - dr/f(r)$, Eq. (3.1) is written as

$$ds^2 = -f(r)du^2 - 2dudr + h(r) \left(d\theta^2 + \sin^2\theta d\phi^2 \right). \tag{3.4}$$

The inverse metric components of the line element (3.4) can be decomposed using the null tetrad $Z^\mu{}_\alpha = (l^\mu, n^\mu, m^\mu, \bar{m}^\mu)$ as

$$g^{\mu\nu} = -l^\mu n^\nu - l^\nu n^\mu + m^\mu \bar{m}^\nu + m^\nu \bar{m}^\mu, \tag{3.5}$$

where

$$l^\mu = \delta^\mu{}_r, \quad n^\mu = \delta^\mu{}_u - \frac{f}{2}\delta^\mu{}_r, \quad m^\mu = \frac{1}{\sqrt{2h}} \left(\delta^\mu_\theta + \frac{i}{\sin\theta}\delta^\mu_\phi \right). \tag{3.6}$$

Using the complex transformation

$$r \rightarrow r' = r + ia\cos\theta, \quad u \rightarrow u' = u - ia\cos\theta, \tag{3.7}$$

where a is the rotation parameter, and replacing the terms r^2 by $\hat{\rho}^2 = r'r'^* = r^2 + a^2\cos^2\theta$ and $\frac{2}{r}$ by $(\frac{1}{r'} + \frac{1}{r'^*}) = \frac{2r}{\hat{\rho}^2}$, we get the new metric in the Eddington-Finkelstein coordinates [17, 24]

$$ds^2 = -F(r,\theta)du^2 - 2dudr + 2a\sin^2\theta \left[F(r,\theta) - 1 \right] dud\phi + 2a\sin^2\theta drd\phi$$
$$+ H(r,\theta)d\theta^2 + \sin^2\theta \left[H(r,\theta) + a^2\sin^2\theta(2 - F) \right] d\phi^2, \tag{3.8}$$

where $F(r,\theta)$ and $H(r,\theta)$ are complexified forms of $f(r)$ and $h(r)$ respectively. In our case using Eqs. (3.2), (3.3) we get

$$f(r) \rightarrow F(r,\theta) = \left(1 - \frac{2(d+M)r}{\hat{\rho}^2} + \frac{2P^2 - k^2}{\hat{\rho}^2} \right) \left(1 - \frac{2dr}{\hat{\rho}^2} - \frac{k^2}{\hat{\rho}^2} \right)^{-1}, \tag{3.9}$$

$$h(r) \rightarrow H(r,\theta) = \hat{\rho}^2 \left(1 - \frac{2dr}{\hat{\rho}^2} - \frac{k^2}{\hat{\rho}^2} \right). \tag{3.10}$$

In Boyer-Lindquist coordinates, the new metric Eq. (3.8) for the rotating black hole finally takes the form [17]

$$ds^2 = -Fdt^2 - 2a(1 - F)\sin^2\theta dtd\phi + \frac{H}{FH + a^2\sin^2\theta}dr^2 + Hd\theta^2$$
$$+ \sin^2\theta \left[H + a^2\sin^2\theta(2 - F) \right] d\phi^2. \tag{3.11}$$

8

After simplification using the explicit forms of $F(r, \theta)$ and $H(r, \theta)$ in our case, we arrive at the line element for a rotating dyonic black hole in Boyer-Lindquist coordinates

$$ds^2 = -\left(1 - \frac{2M(r-d) - P^2 - Q^2}{\hat{\Sigma}}\right) dt^2 - \frac{2a\sin^2\theta}{\hat{\Sigma}}(2M(r-d) - P^2 - Q^2)dtd\phi$$
$$+ \left(r^2 - 2dr - k^2 + a^2 + \frac{a^2\sin^2\theta}{\hat{\Sigma}}\left(2M(r-d) - P^2 - Q^2\right)\right)\sin^2\theta d\phi^2 + \frac{\hat{\Sigma}}{\hat{\Delta}}dr^2 + \hat{\Sigma}d\theta^2 \tag{3.12}$$

where the functions $\hat{\Delta}(r)$ and $\hat{\Sigma}(r, \theta)$ are

$$\hat{\Delta} = r^2 - 2dr - 2M(r-d) - k^2 + a^2 + P^2 + Q^2, \tag{3.13}$$

and

$$\hat{\Sigma} = r^2 - 2dr - k^2 + a^2\cos^2\theta. \tag{3.14}$$

This metric was already derived in [25], [26] using a different method. This is known as the dyonic Kerr-Sen black hole spacetime. Here M and a are the mass and rotation parameters of the black hole. Q and P are the electric and magnetic charges, respectively. $d = (P^2 - Q^2)/2M$ and $k = PQ/M$ are the dyonic charge and axion charge respectively. If the magnetic charge of the black hole vanishes, i.e. $P = 0$ then it reduces to the Kerr-Sen black hole. For the special case, $P = Q$, the dyonic charge vanishes, i.e. $d = 0$, but axion charge $k \neq 0$. This is a distinguishing feature of dyonic Kerr-Sen black holes.

There is a curvature singularity at $r = 0$ covered by the radius

$$r_\pm = M + \frac{P^2 - Q^2}{2M} \pm \sqrt{\left(M - \frac{P^2 + Q^2}{2M}\right)^2 - a^2}. \tag{3.15}$$

The corresponding event horizon and Cauchy horizon are given by $R_+ = \sqrt{r_+^2 - 2dr_+ - k^2}$ and $R_- = \sqrt{r_-^2 - 2dr_- - k^2}$ respectively. The horizon can exist only for

$$\left(1 - \frac{Z_c^2}{2M^2}\right)^2 \geq \frac{a^2}{M^2}, \tag{3.16}$$

where $Z_c^2 = P^2 + Q^2$. Otherwise, the spacetime describes a naked singularity. This is illustrated in Fig. 2.
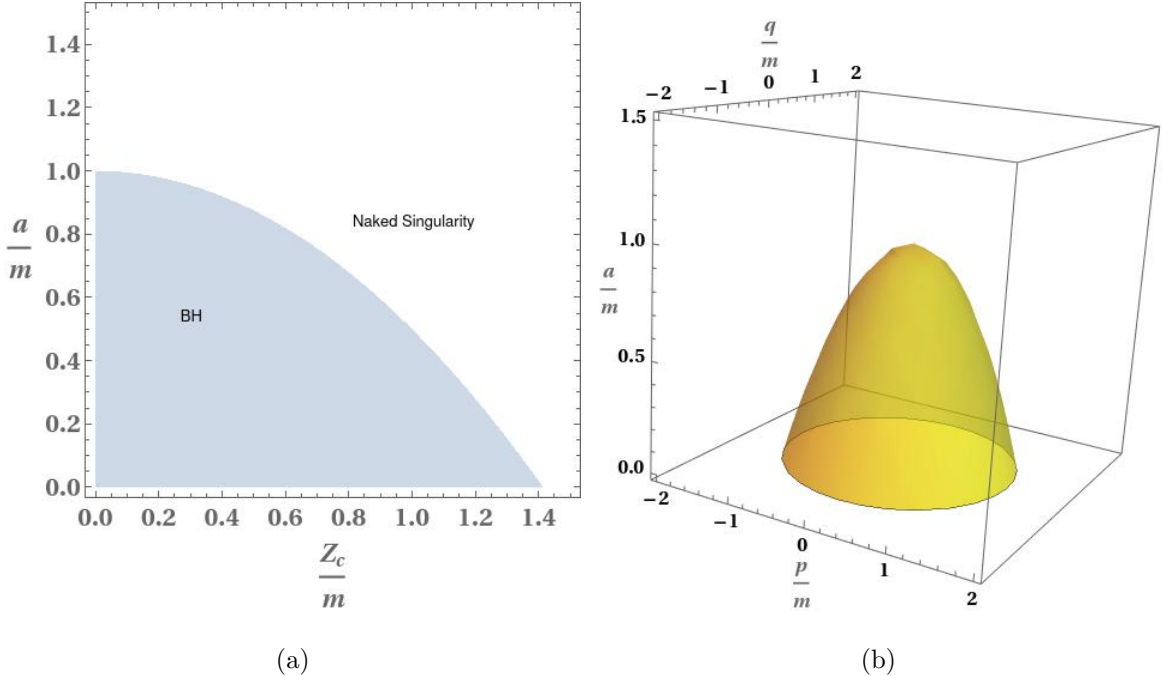
(a)   (b)

FIG. 2: In (a) the shaded region in the a/M- Z_c parameter space corresponds to black holes. In (b) the plot is extended into the full 3-D parameter space of a/M, P/M, and Q/M. Note that $Z_c^2 = P^2 + Q^2$.

IV.   BLACK HOLE SHADOWS

In this section we study the shadow cast by the black holes (both rotating and non-rotating) on the observer's sky. In order to separate the radial (r) and angular (θ) equation of motion for photons, we use the Hamilton-Jacobi method. For the rotating case we use the Boyer-Lindquist coordinates, while for the non-rotating case Schwarzschild coordinates are used.

A.   Shadows of (rotating) dyonic Kerr-Sen black holes

The Hamilton-Jacobi (HJ) equation for photon trajectories is given by

$$H(x^\mu, p_\mu) + \frac{\partial S}{\partial \lambda} = 0 \qquad (4.1)$$

where $S(x^\mu, \lambda)$ is the Jacobi action, λ is the affine parameter, and $H(x^\mu, p_\mu)$ is the Hamiltonian corresponding to the Lagrangian null trajectories given by $\mathcal{L} = \frac{1}{2}g_{\mu\nu}\dot{x}^\mu\dot{x}^\nu = 0$, and 'dot'

10

represents the derivative with respect to the affine parameter λ. The conjugate momentum is $p_\mu = \frac{\partial S}{\partial x^\mu} = \frac{\partial \mathcal{L}}{\partial \dot{x}^\mu}$.

We can write S, using separation of variables, as

$$S = -Et + L\phi + S^r(r) + S^\theta(\theta), \tag{4.2}$$

where $E = -p_t$ and $L = p_\phi$ are the constants of motion. As S does not depend explicitly on λ, the HJ equation becomes $H = \frac{1}{2} g^{\mu\nu} p_\mu p_\nu = 0$. Using $p_r = \frac{\partial S}{\partial r} = \frac{\mathrm{d}S^r}{\mathrm{d}r}$ and $p_\theta = \frac{\partial S}{\partial \theta} = \frac{\mathrm{d}S^\theta}{\mathrm{d}\theta}$ and the inverse metric components

$$g^{tt} = -\frac{(r^2 - 2dr - k^2 + a^2)^2 - \hat{\Delta} a^2 \sin^2\theta}{\hat{\Sigma}\hat{\Delta}}, \tag{4.3}$$

$$g^{t\phi} = g^{\phi t} = -\frac{a}{\hat{\Sigma}\hat{\Delta}}\left(2M(r - d) - P^2 - Q^2\right), \tag{4.4}$$

$$g^{\phi\phi} = \frac{\hat{\Delta} - a^2 \sin^2\theta}{\hat{\Sigma}\hat{\Delta}\sin^2\theta}, \tag{4.5}$$

$$g^{rr} = \frac{\hat{\Delta}}{\hat{\Sigma}}, \quad g^{\theta\theta} = \frac{1}{\hat{\Sigma}}, \tag{4.6}$$

we expand the HJ equation and obtain the separated angular and radial equations of motion of photons. The angular equation of motion is

$$\begin{aligned}
\frac{\mathrm{d}S^\theta}{\mathrm{d}\theta} &= E\sqrt{\Theta(\theta)} \\
&= E\sqrt{\chi - l^2 \cot^2\theta + a^2 \cos^2\theta},
\end{aligned} \tag{4.7}$$

where $\chi = C/E^2$ (C is the Carter constant) and $l = L/E$. The radial equation is

$$\frac{\mathrm{d}S^r}{\mathrm{d}r} = E\sqrt{-V(r)}, \tag{4.8}$$

where the effective potential

$$V(r) = \frac{(l - a)^2 + \chi}{\hat{\Delta}} - \frac{(r^2 - 2dr - k^2 + a^2 - al)^2}{\hat{\Delta}^2}. \tag{4.9}$$

For unstable photon orbits $V(r_{ph}) = V'(r_{ph}) = 0$. After simplification, we obtain $l(r_{ph})$ and $\chi(r_{ph})$ as

$$l(r_{ph}) = \frac{1}{a}\left(r_{ph}^2 + a^2 - 2dr_{ph} - k^2 - 4(r_{ph} - d)\frac{\hat{\Delta}(r_{ph})}{\hat{\Delta}'(r_{ph})}\right), \tag{4.10}$$

$$\chi(r_{ph}) = \frac{16(r_{ph} - d)^2 \hat{\Delta}(r_{ph})}{\hat{\Delta}'^2(r_{ph})} - \frac{1}{a^2}\left(r_{ph}^2 - 2dr_{ph} - k^2 - 4(r_{ph} - d)\frac{\hat{\Delta}(r_{ph})}{\hat{\Delta}'(r_{ph})}\right)^2, \tag{4.11}$$

where $\hat{\Delta}(r_{ph})$ and $\hat{\Delta}'(r_{ph})$ can be obtained from Eq. (3.13) . The celestial coordinates for the observer's sky are

$$\alpha = -\frac{l}{\sin\theta_0}, \quad \beta = \pm\sqrt{\Theta(\theta_0)}, \tag{4.12}$$

where θ_0 is the inclination angle . The parametric plot $\alpha(r_{ph})$ versus $\beta(r_{ph})$ using the Eqs. (4.10), (4.11), and (4.12) gives the shadow profile.

In Fig. 3, the comparison between the shadow profiles for different values of a/M, Q/M, and P/M are shown for the Kerr-Newmann, Kerr-Sen, and dyonic Kerr-Sen black holes. We note that as we increase the P/M values the deviations from the Kerr-Sen and the Kerr-Newmann black holes are more prominent. However, as the a/M value (rotation parameter) is increased the maximum deviation from the Kerr-Sen black holes is found to decrease. This is more prominent in Fig. 4, where all the shadow boundaries approach the outermost black solid curve for the Kerr black holes, as the rotation parameter value is increased.

B. Shadows of static black holes

Using the line element [Eq. (2.7)] for static black holes, the equations of motion for the photon trajectories are

$$\frac{\mathrm{d}S^\theta}{\mathrm{d}\theta} = E\sqrt{\chi - l^2\cot^2\theta}, \tag{4.13}$$

$$\frac{\mathrm{d}S^R}{\mathrm{d}R} = E\sqrt{-V(R)}, \tag{4.14}$$

where $\chi = C/E^2$, $l = L/E$, C is Carter constant, L is angular momentum. The effective potential for the radial equation of motion

$$V(R) = \frac{\psi^2}{\Delta^2}\left[\frac{\chi + l^2}{R^2} - \frac{1}{\Delta^2}\right]. \tag{4.15}$$

For the photon sphere radius (corresponding to the unstable orbits), $V(R_{ph}) = V'(R_{ph}) = 0$, which leads to the relation

$$R_{ph} = \frac{\Delta(R_{ph})}{\Delta'(R_{ph})}. \tag{4.16}$$

Using the expression of $\Delta(R)$ [Eq. (2.20)], we obtain a quadratic equation

$$x^2 + bx + c = 0,$$

$$\text{where,} \quad b = \frac{\tilde{Z}_c^4}{4} + 4\tilde{Z}_c^2 - 9, \tag{4.17}$$

$$\text{and,} \quad c = \tilde{Z}_c^6 - 2\tilde{Z}_c^4,$$

(a)$a/M = 0.5$, $Q/M = 0.85$, $P/M = 0.25$ (b)$a/M = 0.5$, $Q/M = 0.85$, $P/M = 0.35$ (c)$a/M = 0.5$, $Q/M = 0.85$, $P/M = 0.45$

(d)$a/M = 0.65$, $Q/M = 0.75$, $P/M = 0.20$ (e)$a/M = 0.65$, $Q/M = 0.75$, $P/M = 0.25$ (f)$a/M = 0.65$, $Q/M = 0.75$, $P/M = 0.35$
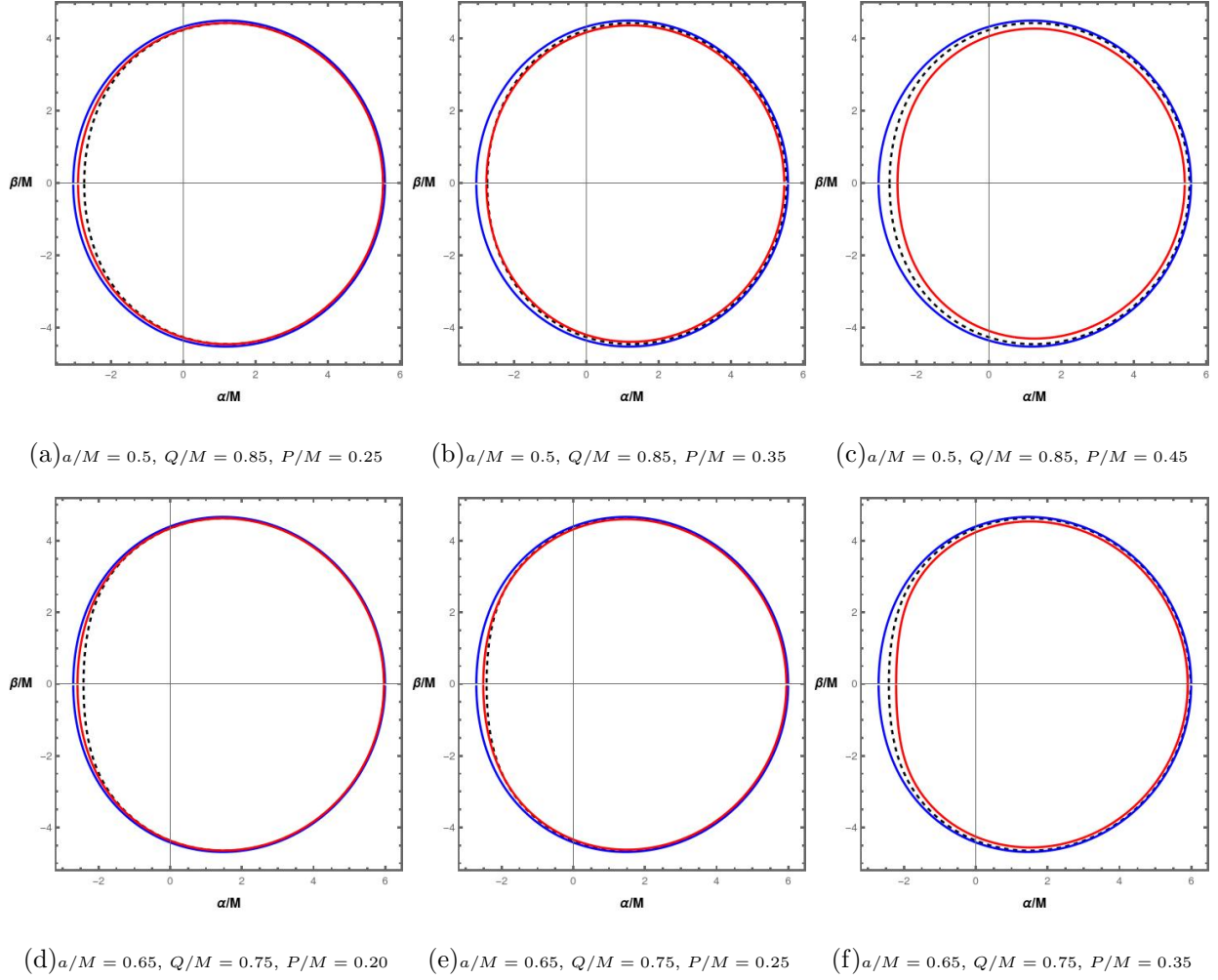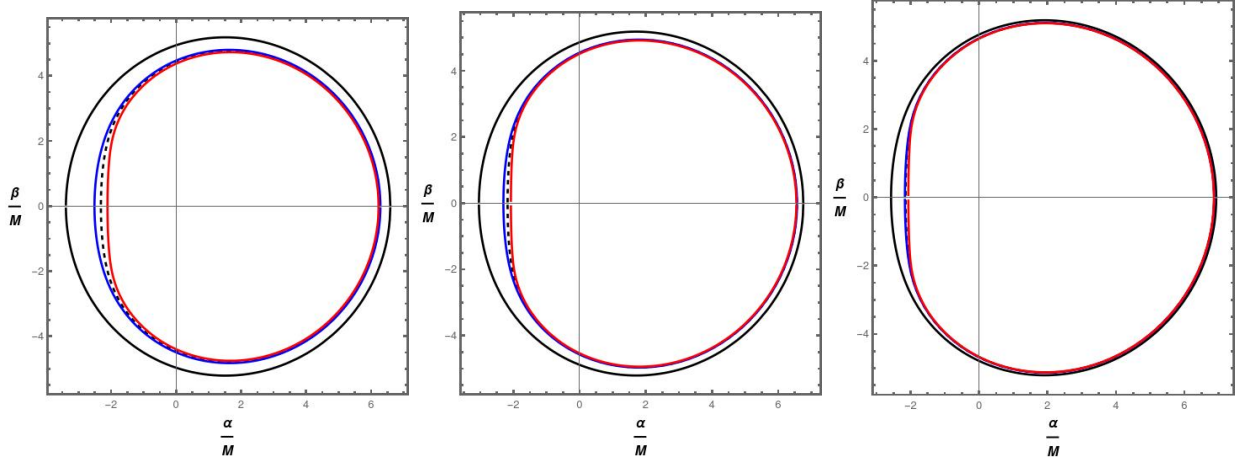
FIG. 3: Shadow boundaries are plotted in the observer's sky, i.e. $\frac{\alpha}{M}$ vs $\frac{\beta}{M}$ space. The black dashed and the solid blue curves in each figure denote the shadow boundaries of the Kerr-Newmann and the Kerr-Sen black holes respectively. The solid red curve denotes the dyonic Kerr-Sen black holes. In the top panel, $a/M = 0.5$ and $Q/M = 0.85$ for all three figures ((a), (b), (c)) but P/M increases for the dyonic Kerr-Sen black holes as we go from (a) to (c). In the bottom panel, the a/M value is increased to $a/M = 0.65$ for the figures (d) to (f). The Q/M value is also fixed at $Q/M = 0.75$ but P/M values are increased for dyonic Kerr-Sen black holes as in the top panel figures. The inclination angle $\theta_0 = 90$ degrees for all the figures.

(a) $a/M = 0.75$, $Q/M = 0.65$, $P/M = 0.27$ (b) $a/M = 0.85$, $Q/M = 0.52$, $P/M = 0.165$ (c) $a/M = 0.95$, $Q/M = 0.30$, $P/M = 0.09$

FIG. 4: Shadow boundaries are plotted in the observer's sky, i.e. $\frac{\alpha}{M}$ vs $\frac{\beta}{M}$ space. The black dashed and the solid blue curves in each figure denote the shadow boundaries of the Kerr-Newmann and the Kerr-Sen black holes respectively. The solid red curve denotes values for the dyonic Kerr-Sen black holes. The outer black solid curve is for Kerr black holes with corresponding rotation parameter (a/M) value. The inclination angle $\theta_0 = 90$ degrees for all the figures.

where $x = R_{ph}^2/M^2$ and $\tilde{Z}_c^2 = (P^2 + Q^2)/M^2$. Then we obtain the photon radius from the root of the quadratic equation, i.e.

$$ x = \frac{R_{ph}^2}{M^2} = \frac{-b + \sqrt{b^2 - 4c}}{2}. \tag{4.18} $$

For the celestial coordinates α and β as defined earlier [Eq. (4.12)] with $a = 0$, we obtain

$$ \alpha^2 + \beta^2 = \chi + l^2 = \frac{R_{ph}^2}{\Delta^2(R_{ph})} = \frac{1}{\Delta'^2(R_{ph})}. \tag{4.19} $$

Therefore the shadow radius for static black holes is

$$ R_{shadow} = \frac{R_{ph}}{\Delta(R_{ph})} $$
$$ = M \left[\frac{x^2}{x - 2\sqrt{x + \frac{\tilde{Z}_c^4}{4}} + \tilde{Z}_c^2} \right]^{1/2}, \tag{4.20} $$

where x is given by Eq. (4.18). For the critical value $\tilde{Z}_c^2 = 2$ the photon-sphere radius vanishes ($R_{ph} = 0$) but the shadow radius does not vanish ($R_{shadow} = 2M$). Thus, the

shadow does not exist for naked singularities. For, $P = Q = 0$, i.e. $\tilde{Z}_c = 0$, $R_{shadow} = 3\sqrt{3}M$, which is the case for the Schwarzschild black hole.

V.   OBSERVATIONAL BOUND ON ROTATING BLACK HOLES

We can test the possible existence of rotating dyonic Kerr-Sen black holes using the observations of black hole shadows of M87* and Sgr A*. To do this, we may define two observational quantities which are– (i) deviation from circularity (ΔC) [27] and (ii) fractional deviation parameter (δ) related to the average shadow diameter [12, 28]. These two quantities are described as follows.

We note that the shadow profile is symmetric about $\beta = 0$, i.e. the α axis. Geometric centre of the shadow image on the α- axis is obtained by taking its mean. Therefore, the centre of the shadow profile is

$$\alpha_c = \frac{\int \alpha \, dA}{\int dA}, \qquad \beta_c = 0, \tag{5.1}$$

where $dA = 2\beta d\alpha$ is the area element on the shadow image. From the geometric centre of the shadow image, the radial distance $\ell(\phi)$ to any point on the shadow boundary, making an angle ϕ with respect α- axis, can be expressed as

$$\ell(\phi) = \sqrt{(\alpha(\phi) - \alpha_c)^2 + \beta(\phi)^2}. \tag{5.2}$$

Then the average shadow radius can be defined as the root mean squared radius, i.e.

$$R_{avg}^2 = \frac{1}{2\pi} \int_0^{2\pi} d\phi \ell^2(\phi). \tag{5.3}$$

Finally, the deviation from circularity is defined as [27]

$$\Delta C = \frac{1}{R_{avg}} \sqrt{\frac{1}{2\pi} \int_0^{2\pi} d\phi \left(\ell(\phi) - R_{avg}\right)^2}. \tag{5.4}$$

For the computation, it is more convenient to use r_{ph} as the parameter instead of ϕ. Then, we can express R_{avg} and ΔC as

$$R_{avg}^2 = \frac{1}{\pi} \int_{r_{ph+}}^{r_{ph-}} (\beta'(\alpha - \alpha_c) - \beta\alpha') \, dr_{ph}, \tag{5.5}$$

$$\Delta C = \frac{1}{R_{avg}} \sqrt{\frac{1}{\pi} \int_{r_{ph+}}^{r_{ph-}} (\beta'(\alpha - \alpha_c) - \beta\alpha') \left(1 - \frac{R_{avg}}{\ell}\right)^2 \, dr_{ph}}, \tag{5.6}$$

where $\beta' = \frac{d\beta}{dr_{ph}}$ and $\alpha' = \frac{d\beta}{dr_{ph}}$. Here r_{ph+} and r_{ph-} are obtained from the roots of $\beta(r_{ph}) = 0$, i.e. the values of r_{ph} for which the shadow boundary cuts the α-axis. In other words, $\phi(r_{ph+}) = 0$ and $\phi(r_{ph-}) = \pi$. The geometric centre of the shadow (α_c, β_c) can also be expressed in terms of the parameter r_{ph} as

$$\alpha_c = \frac{\int_{r_{ph+}}^{r_{ph-}} \alpha\beta\alpha' dr_{ph}}{\int_{r_{ph+}}^{r_{ph-}} \beta\alpha' dr_{ph}}, \qquad \beta_c = 0. \tag{5.7}$$

Note that $\alpha(r_{ph})$, $\beta(r_{ph})$ are obtained from the Eqs. (4.10), (4.11), and (4.12).

From the observation of shadow of M87*, the EHT collaboration has given a bound $\Delta C \lesssim 0.1$ for an inclination angle $\theta_0 = 17^o$ [8–10]. However, the bound on ΔC from SgrA* is not available. From Fig. 5(a), we note that for Kerr black holes the maximum value $\Delta C \lesssim 0.07$ for all inclination angle (θ_0). Considering the orientation of the observed relativistic jets from the M87*, the inclination angle is estimated to be $\theta_0 = 17^o$ [29]. In Fig. 5(b), the variation of ΔC is shown as the function of a/M. Note that the maximum value of $\Delta C \lesssim 0.005$ for the inclination angle $\theta_0 = 17^o$. For the same inclination angle, we scanned the parameter space $a/M - Z_c/M$ for the dyonic Kerr-Sen black holes. From the Fig. 6(a) we note that the for $\Delta C \lesssim 0.00534$. As ΔC increases with the inclination angle θ_0, we have also scanned the parameter space for the inclination angle $\theta_0 = 90^o$ in Fig. 6(b). The maximum possible deviation is $\Delta C \lesssim 0.072$. Therefore, we conclude that all black hole parameters are allowed and the present observational bound on the deviation from circularity cannot constrain the parameter space of the dyonic Kerr-Sen black holes.

The recent EHT papers on SgrA* observations have used the fractional deviation parameter δ to constrain the spacetime geometries different from the Schwarzschild or Kerr black holes. The definition of δ is as follows

$$\delta = \frac{d_{sh}}{d_{sh,Sch}} - 1 = \frac{R_{avg}}{3\sqrt{3}M} - 1, \tag{5.8}$$

where the average diameter of the shadow , $d_{sh} = 2R_{avg}$. Using the observations of the shadow of SgrA* and two separate set of prior values of mass and distance of SgrA* from the VLTI and Keck observations, the EHT collaboration provided the bound on δ [11, 12] as

$$\delta = \begin{cases} -0.08^{+0.09}_{-0.09} & \text{(VLTI)} \\ -0.04^{+0.09}_{-0.10} & \text{(Keck)} \end{cases} \tag{5.9}$$

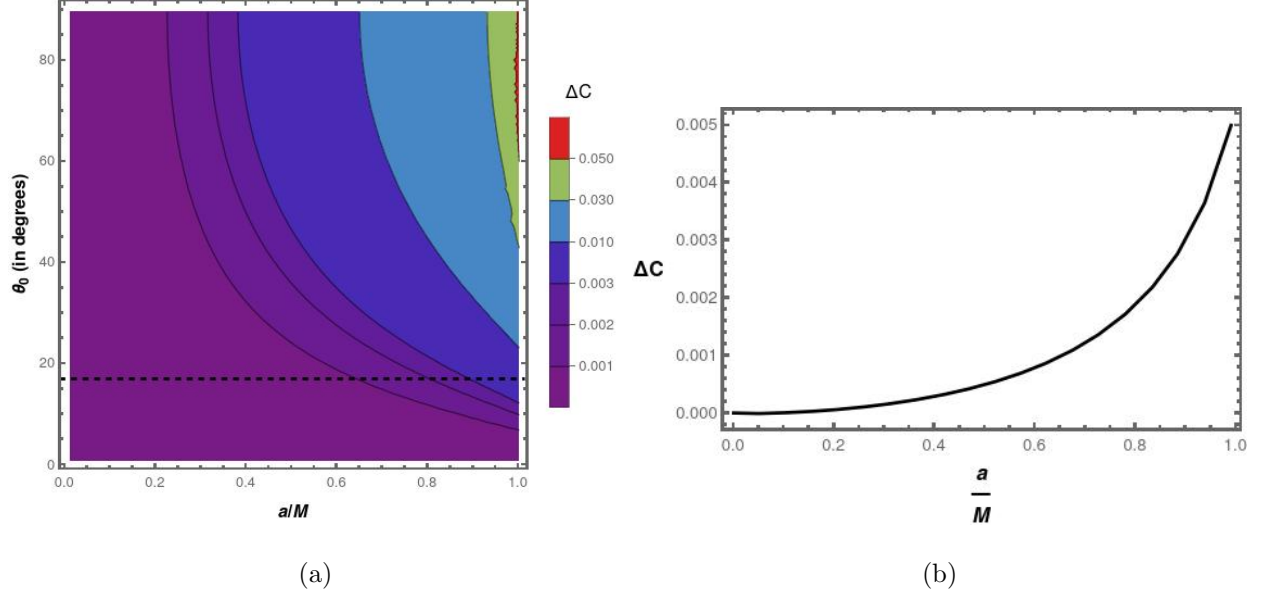(a)   (b)

FIG. 5: (a) The contour plots for different values of ΔC is shown over a/M vs. θ_0 parameter space, for Kerr black holes. The black dashed line corresponds to $\theta_0 = 17^o$. (b) ΔC is plotted as a function of a/M for the inclination angle $\theta_0 = 17^o$.

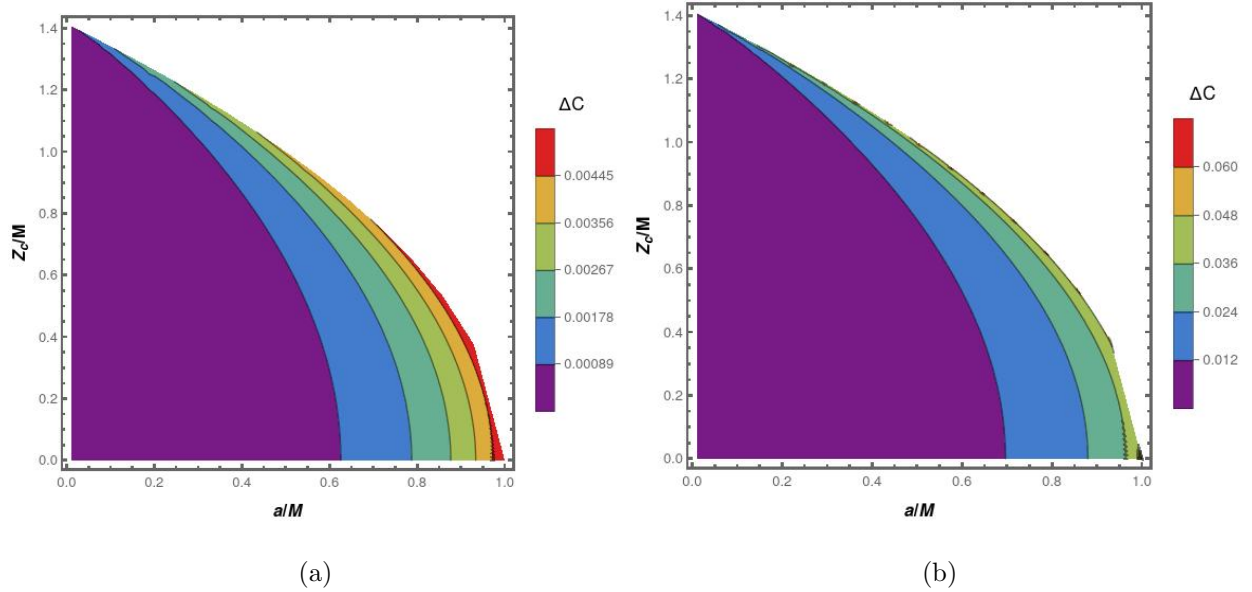(a)   (b)

FIG. 6: The contour plots for different values of ΔC is shown over a/M vs. Z_c/M parameter space for dyonic Kerr-Sen black holes. For plot (a) the inclination angle is $\theta_0 = 17^o$ and for plot (b) $\theta_0 = 90^o$. In the plots, $Z_c = \sqrt{P^2 + Q^2}$. The white excluded region of the parameter space is for naked singularities.
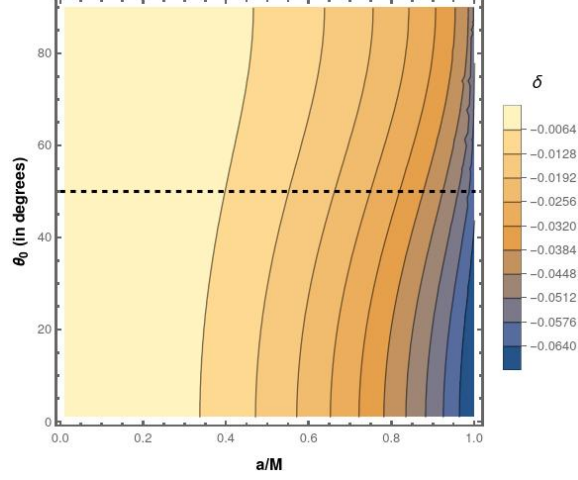
FIG. 7: The contour plots for different values of δ is shown over a/M vs. θ_0 parameter space, for Kerr black holes. The black dashed line corrspends to $\theta_0 = 50^o$.

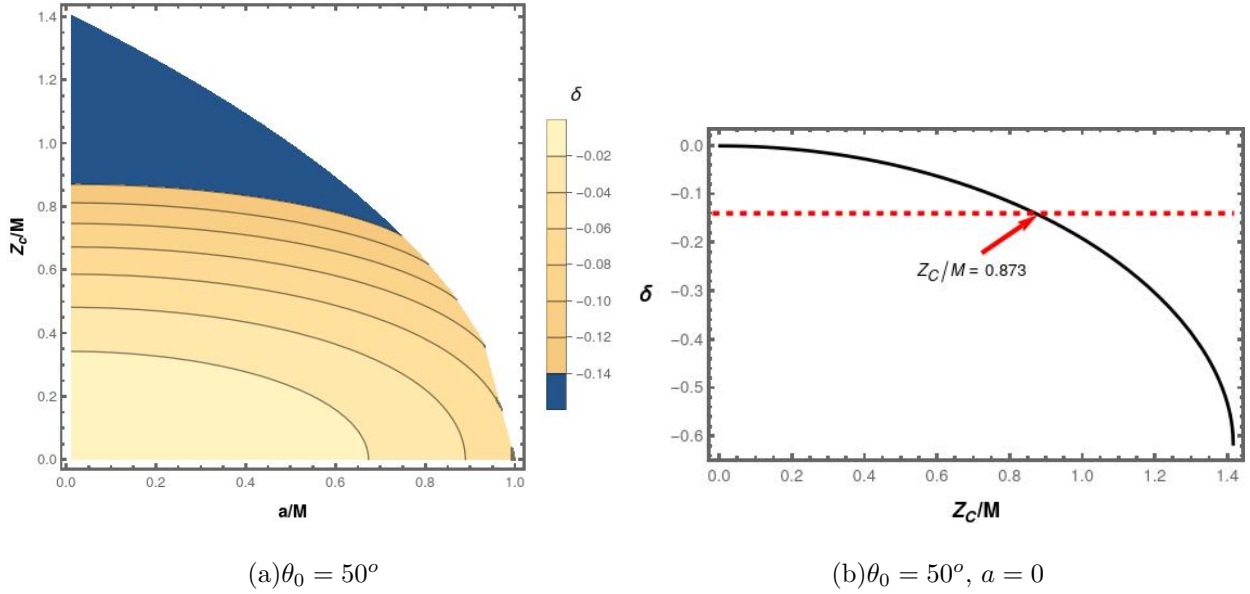(a)$\theta_0 = 50^o$

(b)$\theta_0 = 50^o$, $a = 0$

FIG. 8: (a) The contour plots for different values of δ is shown over a/M vs. Z_c/M parameter space for dyonic Kerr-Sen black holes. The inclination angle is $\theta_0 = 50^o$. The blue shaded region is observationally disfavored as there $\delta < -0.14$. (b) The black solid line is the plot of δ as the function of Z_c/M for static black holes, i.e. $a = 0$. The red dashed line corresponds to $\delta = -0.14$ (the observational limit). It intersects the black solid curve at $Z_C/M = 0.873$, meaning $Z_C/M \lesssim 0.873$ to satisfy the observational constraint.

18

Therefore, combining both these bounds, we have $-0.14 < \delta < 0.01$.

In Fig. 7, we scan the parameter space $a/M - \theta_0$ with the contours labelled by different values of δ for the Kerr black holes. It is noted that $-0.0704 \lesssim \delta < 0$ for all parameter values. Thus, the Kerr black hole parameters are unconstrained from the observational bound on δ from SgrA*. Further, we note that the variation in δ is less sensitive to the variation of θ_0. Moreover, in the observation of SgrA*, inclination angle greater than 50° is disfavored.

Therefore, we choose $\theta_0 = 50^o$ in the Fig. 8(a), where we scan the parameter space $a/M - Z_c/M$ with contours of different δ values for the dyonic Kerr-Sen black holes. In the blue shaded region of the plot $\delta < -0.14$ which means the parameter values $(a/M, Z_c/M)$ are not allowed according to the observations of the SgrA*. Further, we note that for a Z_c/M parameter value greater than the critical limit 0.873, any a/M parameter value does not satisfy the observational constraint. This critical value of Z_c/M parameter is independent of the inclination angle θ_0 as the critical limit corresponds to the $a = 0$, i.e. the static black holes. In Fig. 8(b), we show the variation of δ as the function of Z_c/M for static black holes using the analytical expression for the shadow radius given in Eq. (4.20). There, we explicitly show the critical limit of Z_c/M. We conclude that $Z_c/M \lesssim 0.873$ and for any of allowed Z_c/M parameter value, the allowed range of a/M parameter values must be in the allowed region of space shown in Fig. 8(a).

VI. DISCUSSION AND CONCLUSIONS

In this paper we have revisited black holes with dyonic charges in Einstein-Maxwell-Dilaton-Axion (EMDA) theory in the context of the observations on shadows of the super-massive black holes M87* and SgrA*.

First we outlined the derivation of the static black hole solution by direct integration of the field equations of EMDA theory. Further, the rotating version (the dyonic Kerr-Sen black hole) was obtained from the static solution by applying the Newman-Janis algorithm. Thereafter, we analyzed the structure of the static black holes in detail. The differences with the standard Reissner-Nordström (RN) black holes are parametrized by the quantity $Z_c^2 = P^2 + Q^2$. These static black holes have a single horizon (the event horizon) unlike non-extremal RN black holes. For either $P = 0$ or $Q = 0$ the axion field vanishes. However

the dilaton field vanishes only when both $P = 0$ and $Q = 0$, which is the case for the Schwarzschild black hole. Thus there is no solution with only axion and Maxwell's electromagnetic field but without dilaton field. The reason lies in the structure of the EMDA action where the axion field is linearly coupled with $F_{\mu\nu}\tilde{F}^{\mu\nu}$. The static dyonic black holes satisfy all energy conditions outside the event horizon. There is also no stable photon orbit outside the event horizon of these static dyonic black holes.

For the rotating case ($a \neq 0$) the axion field is non-zero even if the axion charge is zero ($k = PQ/M = 0$) which is the case for the Kerr-Sen black hole ($P = 0$, $Q \neq 0$, and $a \neq 0$). In the static limit of the Kerr-Sen black holes (i.e. setting $a = 0$), the axion field vanishes. This is an interesting difference between the Kerr-Sen black holes and the dyonic Kerr-Sen black holes, in general.

We study the shadow profiles for both rotating and static black holes. We have obtained the exact expression for the shadow radius for static black holes. The parameter $Z_c < \sqrt{2}M$ and the shadow radius R_{shadow} obeys $2M < R_{shadow} < 3\sqrt{3}M$. The effect of magnetic charge/ monopole on the shadow profile of rotating black holes has been investigated graphically by comparing the dyonic Kerr-Sen black holes with the Kerr-Newman and the Kerr-Sen black holes (Fig. 3). The deviation increases with the increase in magnetic charge. However, the deviation is not so prominent for higher rotation parameter (Fig. 4).

Finally, we test whether the known supermassive black holes at galactic centres could be modeled as such dyonic Kerr-Sen black holes. In other words, we look for metric parameter values for which the shadow features match with those in the observed shadow images of M87* and SgrA*. We have used two observational quantities related to black hole shadows – (i) the deviation from circularity of the observed shadow boundary (ΔC) and (ii) the fractional deviation parameter (δ) representing the deviation of the observed average shadow diameter from that for a Schwarzschild black hole. The observational bound on ΔC for M87* is satisfied for all parameter values for the dyonic black holes. Thus, it cannot be constrained. For SgrA*, the EHT collaboration provided a bound on δ which gives a constraint on the black hole parameter $Z_c = \sqrt{P^2 + Q^2} \lesssim 0.873M$. Thus we get an upper bound on the magnetic monopole charge (if any) for SgrA* as $P \lesssim 0.873M$ where $M = 4.154 \times 10^6 M_\odot$ for SgrA*. In natural units, a magnetic charge $Q_m = P/m_P$ where $m_P = G^{-1/2} = 1.22 \times 10^{19}$ GeV is the Planck mass. In these units, the obtained bound on the magnetic charge of SgrA* is $Q_m \lesssim 6.955 \times 10^{44}$.

Magnetic monopoles are a natural outcome of grand-unified theories (GUTs) [30] and was an original motivation for cosmic inflation [31, 32]. They have been searched in various experiments [33–35]. Primordial black holes with magnetic charges, which reached the extremality condition in due course of cosmic evolution and do not Hawking radiate anymore, can be a possible dark matter candidate [36]. They are termed as the extremal Magnetic Black Holes (EMBHs). Various astrophysical limits on such EMBHs was discussed in [36]. However, the authors put constraints on the black holes with mass range having the upper limit $M < 10^{33}\, g$. Therefore these black holes cannot be modeled as the supermassive black holes like M87* and SgrA* and thus cannot be directly compared with the bound that we obtained from the observations of shadow images. However, we can have some idea on what type of physical process can give bounds on the magnetic charge of the supermassive black holes at the center of our galaxy. For example, from the observed temperature of clouds of Warm Ionized Medium (WIM) in the Milky Way [37], we can put some upper bound on the magnetic charge of SgrA*. Following the calculations of [36], we get a rough estimation on the upper bound on the magnetic charge of SgrA* to be $P \lesssim 10^{-13}M$. Another astrophysical constraint comes from the Parker bound [38] which is based upon the survival of today's galactic magnetic field, as the field energy is drained out by the magnetic monopoles while moving through the field. This puts an upper limit on the flux of magnetic monopoles. From the Parker bound our rough estimate on the magnetic charge of SgrA* is $P \lesssim 359\, M_\odot$ and thus $P/M \lesssim 10^{-4}$. Clearly, the other astrophysical constraints are expected to be far more stringent by several orders of magnitude.

Thus, any possible observational relevance of our results, atleast in the context of shadows and the viable presence of magnetic charges seems quite a distant dream. However, the theoretical analysis we have carried out, may be of use once more imaging observations on shadows of black holes are carried out and presented in future.

ACKNOWLEDGEMENTS

Institute of Technology Kharagpur.

[1] B. Chen and J.-j. Zhang, Phys. Rev. D **87**, 081505 (2013).

[2] G. W. Gibbons and K.-i. Maeda, Nucl. Phys. B **298**, 741 (1988).

[3] D. Garfinkle, G. T. Horowitz, and A. Strominger, Phys. Rev. D **43**, 3140 (1991), [Erratum: Phys.Rev.D 45, 3888 (1992)].

[4] A. Sen, Phys. Rev. Lett. **69**, 1006 (1992), arXiv:hep-th/9204046.

[5] B. A. Campbell, N. Kaloper, and K. A. Olive, Phys. Lett. B **263**, 364 (1991).

[6] A. D. Shapere, S. Trivedi, and F. Wilczek, Mod. Phys. Lett. A **6**, 2677 (1991).

[7] R. Kallosh and T. Ortín, Phys. Rev. D **48**, 742 (1993).

[8] E. H. T. Collaboration, The Astrophysical Journal Letters **875**, L1 (2019).

[9] E. H. T. Collaboration, The Astrophysical Journal Letters **875**, L5 (2019).

[10] E. H. T. Collaboration, The Astrophysical Journal Letters **875**, L6 (2019).

[11] E. H. T. Collaboration, The Astrophysical Journal Letters **930**, L12 (2022).

[12] E. H. T. Collaboration, The Astrophysical Journal Letters **930**, L17 (2022).

[13] K. Hioki and U. Miyamoto, Phys. Rev. D **78**, 044007 (2008), arXiv:0805.3146 [gr-qc].

[14] S. V. M. C. B. Xavier, P. V. P. Cunha, L. C. B. Crispino, and C. A. R. Herdeiro, Int. J. Mod. Phys. D **29**, 2041005 (2020), arXiv:2003.14349 [gr-qc].

[15] A. Narang, S. Mohanty, and A. Kumar, (2020), arXiv:2002.12786 [gr-qc].

[16] G.-J. Cheng, R.-R. Hsu, and W.-F. Lin, J. Math. Phys. **35**, 4839 (1994), arXiv:hep-th/9302065.

[17] R. Shaikh, Phys. Rev. D **100**, 024028 (2019), arXiv:1904.08322 [gr-qc].

[18] I. Banerjee, S. Sau, and S. SenGupta, (2022), arXiv:2207.06034 [gr-qc].

[19] I. Banerjee, S. Sau, and S. SenGupta, Phys. Rev. D **101**, 104057 (2020), arXiv:1911.05385 [gr-qc].

[20] M. Cvetič, G. W. Gibbons, and C. N. Pope, Phys. Rev. D **94**, 106005 (2016).

[21] G. Guo, Y. Lu, P. Wang, H. Wu, and H. Yang, arXiv **2212.12901** (2022).

[22] E. T. Newman and A. I. Janis, J. Math. Phys. **6**, 915 (1965).

[23] E. T. Newman, E. Couch, K. Chinnapared, A. Exton, A. Prakash, and R. Torrence, Journal of Mathematical Physics **6**, 918 (1965).

[24] S. P. Drake and P. Szekeres, Gen. Rel. Grav. **32**, 445 (2000), arXiv:gr-qc/9807001.

[25] D. V. Gal'tsov and O. V. Kechkin, Phys. Rev. D **50**, 7394 (1994).

[26] D. Wu, S.-Q. Wu, P. Wu, and H. Yu, Phys. Rev. D **103**, 044014 (2021), arXiv:2010.13518 [gr-qc].

[27] C. Bambi, K. Freese, S. Vagnozzi, and L. Visinelli, Phys. Rev. D **100**, 044057 (2019), arXiv:1904.12983 [gr-qc].

[28] R. Shaikh, (2022), arXiv:2208.01995 [gr-qc].

[29] R. C. Walker, P. E. Hardee, F. B. Davies, C. Ly, and W. Junor, The Astrophysical Journal **855**, 128 (2018).

[30] G. Hooft, Nuclear Physics B **79**, 276 (1974).

[31] A. H. Guth, Phys. Rev. D **23**, 347 (1981).

[32] J. P. Preskill, Phys. Rev. Lett. **43**, 1365 (1979).

[33] M. Ambrosio et al. (MACRO), Eur. Phys. J. C **25**, 511 (2002), arXiv:hep-ex/0207020.

[34] S. Orito et al., Phys. Rev. Lett. **66**, 1951 (1991).

[35] S. Balestra et al., Eur. Phys. J. C **55**, 57 (2008), arXiv:0801.4913 [hep-ex].

[36] M. D. Diamond and D. E. Kaplan, JHEP **03**, 157 (2022), arXiv:2103.01850 [hep-ph].

[37] N. Lehner, B. P. Wakker, and B. D. Savage, Astrophys. J. **615**, 767 (2004), arXiv:astro-ph/0407363.

[38] E. N. Parker, Astrophys. J. **160**, 383 (1970).